Design and Operational Performance Maps of Calcium Looping Thermochemical Energy Storage for Concentrating Solar Power Plants

S. Pascual [a] *, P. Lisbona [b], M. Bailera [a], L.M. Romeo [a]

[a] Escuela de Ingeniería y Arquitectura. Universidad de Zaragoza, Zaragoza, España

[b] Fundación Agencia Aragonesa para la Investigación y el Desarrollo (ARAID), Zaragoza, España

* Corresponding author.
E-mail address: saraps@unizar.es

Abstract

Calcium-looping thermochemical energy storage associated to concentrating solar plants appears as promising technology given its potential to increase the storage period and energy density of the stored material. Up to now, research efforts focused on the global efficiency of the TCES associated to different power cycles under fixed modes of operation: day or night. However, TCES will never operate under a stationary situation but will experience different operation points to adapt to solar availability and energy demand from the power cycle. The aim is to analyse the influence of those variables which define the operation points, under energy storage and release modes, in the design of the heat exchangers network, storage tanks and reactors involved in the TCES system. The equipment in the conceptual plant have been modelled accounting variable storage/discharge fractions in the mass balances. The results show a suitable capture efficiency, quantifies the stored power and define the size and performance of the heat exchangers required to operate the system. The behaviour of each heat exchanger and their relevance in heat integration with a power plant is derived. The novelty relies in the analysis of potential situations arising from different combinations of charge/discharge fractions of storage tanks.

Keywords

Calcium-looping, Thermochemical energy storage, Concentrated solar power, Energy storage operation mode, Energy release operation mode.

1. Introduction

The dispatch of concentrated solar power (CSP) plants presents a peak around noon, in addition to continuous variations due to cloud coverage, that make energy storage systems necessary to properly manage electricity production. Currently, the 54% of the CSP plants worldwide include thermal energy storage (TES) to increment their daily operating hours and maximize the electricity production [1]. These TES systems retain thermal energy within a specific material and release it when needed. According to the physical phenomena occurring while storing/releasing energy, thermal energy storage is classified in (i) sensible TES, (ii) latent TES and (iii) thermochemical energy storage (TCES).

Sensible TES uses materials with high specific heat (131–4187 J/kg·K) to store/release energy by heating/cooling their mass. Although the energy storage density of these systems is low (1001–4453 kJ/m^3·K), they are simple, reliable and cheap, making them the most widely used TES system in commercial CSP plants [2]. Within sensible TES, molten salts are the most commonly applied materials [3]. Their major drawback is the required range of working

temperatures, since molten salts must be maintained above 200 °C to prevent solidification, and not exceed 550 °C to avoid its degradation [4].

Latent TES uses materials with high latent heat (112–260 kJ/kg) to store/release energy during a liquid-solid phase transition, in order to have constant temperature [2], small variations in volume (<10%) [5] and high energy storage densities (50 to 150 kWh/t). The main disadvantage of latent TES is the prolonged times of charging and discharging energy, because of the low thermal conductivity of these materials (< 0.5 W/m·K) [2].

Thermochemical energy storage uses the reversibility of certain chemical equilibrium reactions (endothermic in one direction and exothermic in the other one) to store/release energy through a cyclic process. TCES system improves storage capacity compared to sensible and latent TES, through the introduction of materials with higher energy density (about 240-1090 kWh/t) [6] and minimal energy loss under seasonal storage since the energy is stored in the chemical bound of the compounds. Furthermore, since TCES operates in the temperature range of 450–1300 ºC, it can also be integrated in new generation CSP plants, which operate above 800 ºC [2][7].

One of the most promising TCES systems is based on the reversible calcination – carbonation reaction of $CaCO_3$/CaO, also known as calcium-looping (CaL) process [8]. Calcination reaction (Eq. (1)) is endothermic, producing carbon dioxide (CO_2) and calcium oxide (CaO) at 920 – 950 ºC [9]. The thermal energy used in the calcination process should be energy intended to be stored or energy that would otherwise be wasted. Both products from calcination reaction can be independently stored until the stored energy is required to be recovered. The exothermic reaction (reverse Eq. (1)) is produced when the stored CO_2 and CaO are mixed at temperatures in the range 600 – 850 ºC [10]. This carbonation reaction releases high temperature heat and produces $CaCO_3$ that can be stored, thus closing the loop.

$$CaCO_{3\,(s)} \leftrightarrows CaO_{(s)} + CO_{2\,(g)} \qquad \Delta H_R^{\circ} = +178\ kJ/mol \qquad (1)$$

CaL process uses limestone ($CaCO_3$), which is a non-toxic, earth-abundant and cheap material (< 10 €/t $CaCO_3$) [11]. Besides, $CaCO_3$ material presents high energy density, in the range 307 – 409 kWh/t [7][12]. The most important drawback of the CaL process is the decay of sorbent capacity of CaO material due to sintering [13], which becomes more relevant the higher is the number of carbonation-calcination cycles suffered by the solid particles [14][15]. This particular problem has been extensively studied in literature looking for different solutions: sorbent improvements by analyzing the multicycle activity of the natural $CaCO_3$ minerals [16], pre-processing limestone to enlarge the long-term performance of the sorbent upon iterated cycles [17], doping and modifying $CaCO_3$ [18][19], and developing synthetic Ca-based materials for energy storage [20].

Although the utilization of CaL for energy storage was already proposed in 1974 by Barker [8], was not until the last decade that several research works analyzed its application in CSP plants. In this case, the calcination reaction would occur during sunlight hours whenever solar energy is available in the CSP. The calcination products (CaO and CO_2) can be total or partially stored, diverting the rest to the carbonator to produce energy. During night period, the stored CO_2 and CaO are always sent to carbonator to produce energy, aiming to keep at least a minimum operating load to avoid expensive shutdowns of the power plant.

The operation of this system is associated with power cycles for electricity production, therefore recent research mainly focus on the selection of the most suitable power block to be integrated with CaL TCES [21][22][23] and the subsequent optimization of the overall efficiency [24][25][26][27]. Also, some authors have studied the design of reactors [9][28] and the management of the storage system [29].

Ortiz et al. [21], Tesio et al. [22] and Karasavvas et al. [23] compared different power cycles aiming for the best performance when integrated with calcium looping TCES. All of them concluded that CO_2 power cycles provide the greatest results (supercritical CO_2 power block

according to Tesio, and CO_2 closed Brayton cycle according to Ortiz and Karasavvas). After identifying the most suitable technology, they optimized the overall efficiency (net electric production to net solar thermal input) by assessing different plant layouts and operating conditions. In the case of supercritical CO_2 cycles, the efficiency was 40.4% [26], while for CO_2 closed Brayton cycle the higher efficiencies of the different authors were within the range 31-44% [24][25][27].

In terms of plant management, Bravo et al. [29] used a multi-objective optimization framework to define the operational strategy that would maximize the net energy supplied during one year of operation. They analyzed 9 potential scenarios, obtaining capacity factors in the range 48 – 69% (referred to the operation of the CO_2 Brayton cycle) and efficiencies between 33.1% and 33.8% (net electric production to net solar thermal input in the calciner).

Although the mentioned studies assume industrial plants, they do not consider the implications that reactor design may have on the overall efficiency at this scale. Only Bailera et al. [28] for carbonation and Lisbona et al. [9] for calcination, have started shedding light on this issue. Bailera et al. showed that carbonators cooled by external coils, when scaled-up to industrial scale, cannot properly evacuate the exothermal energy. Since the reaction gets inhibited, the carbonator dimensions for a 100 MW CSP plant become unreasonable (7 m in diameter and 52 m in length) [28]. Regarding calcination, Lisbona et al. assessed the temperature profile in a falling particle calcinator [9]. In this type of reactors, a curtain of falling $CaCO_3$ particles absorb the solar radiation that enters through the aperture of the receiver [30]. To keep the profile close to isothermal and avoid excessive degradation due to peaks of temperature, they proposed supplying the solar thermal energy through different stages along the calcinator. They concluded that a 3-stage calcinator provides an adequate balance between complexity, energy storage efficiency (98.9%), and temperature variation (895 – 993 ºC) [9]. The main reason of the lack of studies regarding reactor design [31] is that experiments on CaL TCES are scarce. So far, solar calcination has been tested by the Paul Scherrer Institute in a window-less cyclone gas-particle separator with a solar thermal input of 54 kW (85% limestone conversion and 88% energy efficiency) [30], while carbonation is being tested within the SOCRATCES project in a 10 kW entrained flow reactor cooled by air through external coils [32]. Thus, the CaL TCES technology is currently in TRLs 5 – 6, which is in the upper range of similar energy storage technologies based on endothermic-exothermic thermochemical cycles [33].

The research gap found in most of these studies is that they are performed under stationary operation modes of the CaL TCES system. It means that both the fraction of calcination products diverted to storage during sunlight hours and the operating load of the carbonator during night period are fixed values. In this work, not only one single operation point is analyzed at each mode of operation (energy storage and energy release), but a whole scanning of possible operation points is carried out. Therefore, the novelty of the paper is the analysis of the wide variety of potential situations that may take place, arising from the different combinations of charge/discharge fractions of the CaO, CO_2 and $CaCO_3$ storage tanks. Thus, it will cover scenarios such as low/high electricity demands, limited solar energy availability, variations in electricity prices, etc.

The main objective of this study is to determine the required size of the heat exchangers that are present in a CSP plant with CaL TCES under a wide range of potential scenarios, and stablish their operation maps versus the different charge/discharge fractions of the CaO, CO_2 and $CaCO_3$ tanks. The paper is structured in the following way: in section 2, the CSP plant integrated with calcium looping TCES and the energy storage/release operation modes are described; in section 3, the methodology used to model the plant and size the equipment is presented; in section 4, the results on heat exchangers requirements and operation maps are discussed; in section 5, the main conclusions of the study are remarked.

2. Plant description and operation modes

The thermal energy storage capacity of the CaL TCES system proposed in this study is 100 MWth at nominal conditions. As shown in Fig. 1, the system consists of two main reactors, a solar calciner and a carbonator, with intermediate storage tanks of CO_2, CaO and $CaCO_3$. The size and technical characteristics of these elements are described in the following paragraphs.

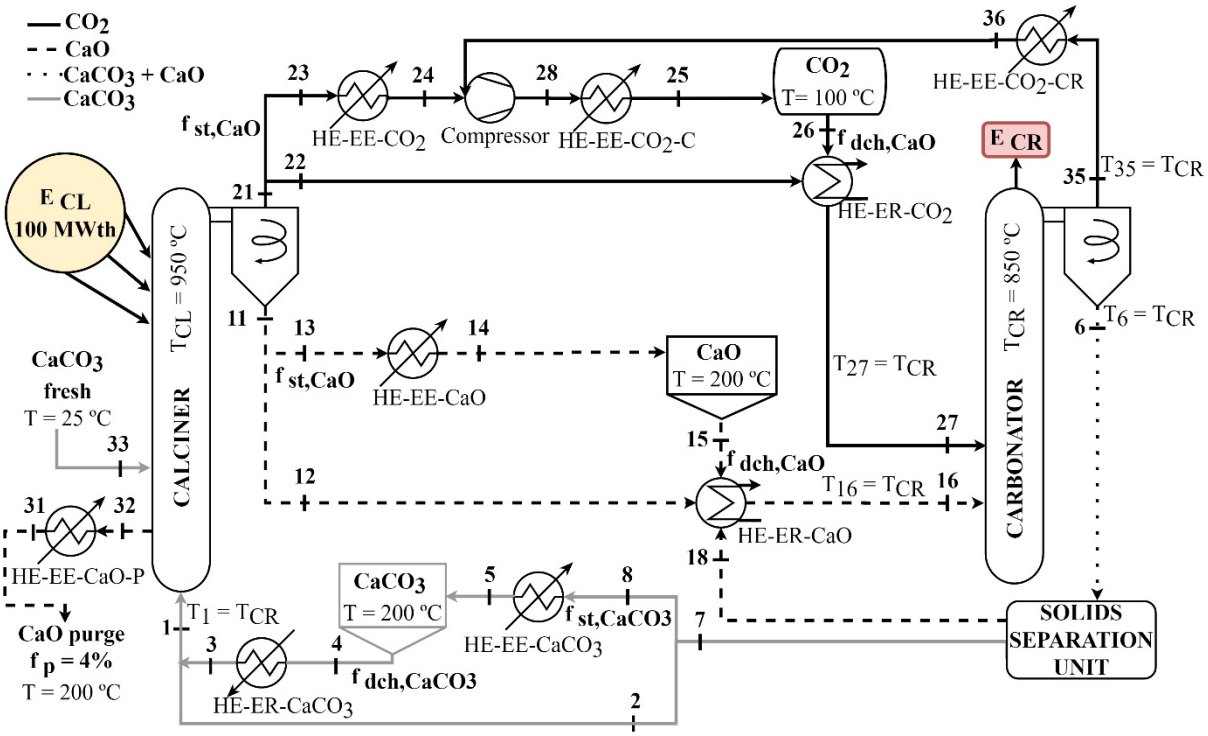

Fig. 1. Thermochemical storage system based on Calcium-looping process for a 100 MWth CSP plant

2.1. Plant description

2.1.1. Concentrated solar power and solar field

The power required in the calciner is supplied by the solar energy captured in a concentration solar field. For this case study, a solar power tower plant located in the same site as the PS10 commercial plant in Seville (Spain) is considered [1]. This location has been selected given the high annual availability of the solar resource and the high solar irradiation. The annual Direct Normal Irradiance considered is 2012 kWh/m^2/year [1]. The calciner is found inside the receiver of the solar power tower. The required solar field area is 250000 m^2, considering an optical efficiency of 64.7% and a thermal efficiency of 92.8% [34]. Taking into account irradiance data from the PVGIS tool [35], the maximum power that could reach the interior of solar receiver would be 155 MW, while the average power during sunlight hours throughout the year is 83 MW. Therefore, it is reasonable to assume a thermal input of 100 MWth to the calciner under nominal operation conditions.

2.1.2. Calciner

The input flowrate of $CaCO_3$ to the calciner (stream 1) results from the addition of the limestone stream from the solids separation unit at 850 °C (stream 2) and the flowrate of $CaCO_3$ discharged from the limestone storage tank at 200 °C (stream 4). The inlet solid stream must be heated up to 850 °C. The calcination or sorbent regeneration process produces

a continuous flowrate of CaO and CO_2, which can be stored (stream 13 and 23) or directed to the carbonator reactor to close the chemical Ca-looping (stream 12 and 22).
Since CaO quickly deactivates with the number of cycles, a stream of fresh limestone must be fed into the calciner to keep a reasonable age population and sorption activity. Besides, the operating temperature in the calciner does not exceed 950 ºC in CO_2 pure atmosphere in order to avoid further degradation of CaO [24]. Therefore, the $CaCO_3$ supplied to the calciner reactor comes from: (i) the contribution of fresh limestone and (ii) the $CaCO_3$ produced after carbonation reaction. Regarding the mass balance in the calciner, fresh limestone (stream 33 or F_0) counterbalances the purged solid material (f_p) which is set at 4% of the CaO molar flow generated in calcination reaction (stream 11 or $F_{CaO,outCL}$), as shown in Eq. (2).

$$f_p = \frac{F_0}{F_{CaO,outCL}} \quad (2)$$

2.1.3. Carbonator

Exothermal carbonation reaction takes place in the carbonator at 850 °C in pure CO_2 atmosphere [36]. Ideally, the carbonator operates in isothermal mode although it is difficult to achieve under normal operation [28]. The CaO stream discharged from the storage tank at 200 ºC (stream 15) is mixed with a CaO stream diverted from the calciner outlet at 950 ºC (stream 12) and a recycled CaO flow rate at 850 ºC from the solids separation unit outlet (stream 18) before being introduced into carbonator at 850 ºC.
The nominal power in the carbonator has been set considering the operation of the CaL facility without storage of materials, i.e. as a single capture cycle, and a heat input to the calciner of 100 MWth. In this case, the nominal power input (100 MWth) is used to calcinate an amount of sorbent which is fully directed to the carbonator to be completely carbonated releasing the maximum potential of thermal energy in this reactor, 88.33 MWth.
It is known that only a percentage of the CaO introduced in the carbonator (stream 16) will react with CO_2 (stream 27). This amount will depend on the average sorption activity of the population of particles circulating in the system [37]. A mixture of $CaCO_3$ and unreacted CaO is found at carbonator outlet (stream 6). To avoid the storage of a mixture of compounds, solid stream leaving the carbonator is completely separated into its two components, CaO and $CaCO_3$, at high temperature (850 ºC). This separation process allows to avoid the subsequent heating and cooling of CaO which otherwise would be directed the calciner and also allows to reduce the $CaCO_3$ storage tank size. The output stream of CaO is recirculated to the carbonator (stream 18), while the flowrate of $CaCO_3$ can be stored (stream 8) or directed to the calciner (stream 2), according to the operation mode. The unreacted CO_2 leaving the carbonator is stored together with the CO_2 from the calciner under established conditions and it will be fed into the carbonator again when required. The value of R and the average sorption activity (X_{ave}) define the carbon capture efficiency (η_{capt}) in the carbonator reactor (Eq. (3)).

$$\eta_{capt} = R \cdot X_{ave} = \frac{F_{CaO,inCR}}{F_{CO2,inCR}} \cdot X_{ave} = \frac{F_{stream\ 16}}{F_{stream\ 27}} \cdot X_{ave} \quad (3)$$

2.1.4. Storage tanks

Temperature and pressure of the CO_2 storage depend on the storage tank size and phase of stored CO_2 [36]. In this study, CO_2 is stored in gas phase at 100 ºC and 73 bar. CO_2 compression process to achieve these storage conditions includes a cooling stage down to 50 °C before compression to 73 bar and a final cooling to the storage temperature, 100 °C. CO_2 from storage tank is mixed with CO_2 from calciner before being introduced into carbonator at 850 ºC. Solids storage temperature may ranges from ambient to 200 – 700 ºC [24]. Solids storage temperature and pressure are set at 200 °C and 1 bar.

2.1.5. Heat exchangers

Heat exchangers (HE) illustrated in Fig. 1 will supply or remove thermal energy according to the operation mode of the overall TCES system. Heat exchangers designated as *EE* are able to provide energy under both modes of operation, storage or release mode. Heat losses of these *EE* heat exchangers are assumed to be a 2% of the power exchanged.
However, the heat exchanger designated as *ER-$CaCO_3$* always requires thermal energy input under any operating situation while the rest of *ER* heat exchangers provide or demand energy depending on the operation mode.

2.2. Operation modes

The management of the flow streams to and from the storage tanks will depend on the availability of renewable energy resource and/or the requirement of releasing thermal energy from the TCES, which will determine the operation mode: energy storage (ESOM) or energy release (EROM). First, storage and discharge fractions must be defined to describe the flows of gas and solids circulating in the system under each operation mode.

2.2.1. Storage and discharge fractions

Stationary operation is analysed in this study for both operation modes considering different combinations of discharge and storage fractions from and to storage tanks. Mapping a wide range of operation points will allow the estimation of the required size ranges of the equipment involved in the system.
The maximum CO_2 flow rate which can be diverted to the storage tank ($\dot{m}_{st,max,CO2}$) would correspond to the CO_2 flow rate leaving the calciner (stream 21) when the thermal energy received is 100 MWth (nominal operation of the solar calciner). The amount of CO_2 received in the storage tank ($\dot{m}_{st,CO2}$) will correspond to a fraction of this maximum CO_2 stream that actually leaves the calciner under nominal conditions ($f_{st,CaO}$), Eq. (4). The CO_2 leaving the storage tank ($\dot{m}_{dch,CO2}$) is defined as a fraction of the maximum possible flowrate of CO_2 at calciner outlet ($f_{dch,CaO}$), Eq. (5).
The maximum CaO flow rate ($\dot{m}_{st,max,CaO}$) which could be sent to the storage tank corresponds to the CaO flowrate leaving the calciner (stream 11) when it is operated at nominal conditions; i.e. solar power received of 100 MWth. The CaO storage tank receives ($\dot{m}_{st,CaO}$) a fraction of this maximum CaO stream produced in the calciner under nominal conditions ($f_{st,CaO}$). The amount of CaO actually discharged from the storage tank ($\dot{m}_{dch,CaO}$) is also defined as a fraction of the maximum possible flow of CaO that leaves calciner ($f_{dch,CaO}$), as shown in Eq. (4) and Eq. (5), respectively. These storage and discharge fractions are analogous to those fractions of CO_2 in order to keep CaO/CO_2 molar ratio (*R*) constant.

$$f_{st,CaO} = \frac{\dot{m}_{st,CaO}}{\dot{m}_{st,max,CaO}} = \frac{\dot{m}_{st,CO2}}{\dot{m}_{st,max,CO2}} \quad (4)$$

$$f_{dch,CaO} = \frac{\dot{m}_{dch,CaO}}{\dot{m}_{st,max,CaO}} = \frac{\dot{m}_{dch,CO2}}{\dot{m}_{st,max,CO2}} \quad (5)$$

The maximum storage flowrate of $CaCO_3$ ($\dot{m}_{st,max,CaCO3}$) corresponds to the $CaCO_3$ flowrate leaving the carbonator (stream 7) when it operates under its nominal conditions, i.e. 88.33 MWth released in this equipment. The maximum $CaCO_3$ stream leaving the solids separation unit located downstream the carbonator can be totally or partially ($\dot{m}_{st,CaCO3}$) diverted to the $CaCO_3$ storage tank ($f_{st,CaCO3}$). On the other hand, the discharge $CaCO_3$ flowrate of this tank ($\dot{m}_{dch,CaCO3}$) is defined as a fraction of the maximum possible flow of $CaCO_3$ leaving the carbonator ($f_{dch,CaCO3}$), as shown in Eq. (6) and Eq. (7), respectively.

$$f_{st,CaCO3} = \frac{\dot{m}_{st,CaCO3}}{\dot{m}_{st,max,CaCO3}} \quad (6)$$

$$f_{dch,CaCO3} = \frac{\dot{m}_{dch,CaCO3}}{\dot{m}_{st,max,CaCO3}} \quad (7)$$

2.2.2. Energy storage operation mode (ESOM)

This operation mode will be activated whenever solar energy is available and becomes an input to the calciner instead to run the CSP plant. This could correspond to CSP daylight operation under very low electricity demand situation. As already defined, the nominal operation of the solar calciner receives 100 MWth. Under the energy storage mode, the CO_2 and CaO flowrates from the calciner are totally or partially directed to the storage tanks. The balance between stored energy and available heat from the system will vary depending on the amount of material directed to storage tank or to carbonator. Since a fraction of the mass streams leaving the calciner is stored and only the remaining part is circulated to the carbonator, the energy available in the carbonator will be correspondingly reduced with respect to nominal operation. The storage tank of limestone will be required to discharge material to feed the calciner and close the mass balance of the system.

2.2.3. Energy release operation mode (EROM)

This operation model will be activated whenever solar input to the calciner is not available but thermal energy is still required in the CSP plant. It could correspond to the operation of the CSP during high electricity demand periods or night hours. Under energy release mode, the received solar energy will always be lower than 100 MWth in the calciner. Thus, limestone flow rate from carbonator must be completely stored when no solar input is available or partially diverted to the calciner when solar power is available. The flow rate of limestone diverted to the calciner will correspond to the amount of limestone which can be potentially calcined using the available solar energy. The storage tanks of CO_2 and CaO will be required to discharge material in order to maintain the energy availability in the carbonator.

3. Materials and methods

This section details the methodology followed for (i) the modelling of the carbonator to obtain the performance parameters of the Ca-looping and (ii) the evaluation of equipment sizing involved in the system according to the operation modes: energy storage or energy release. The model of the carbonator and calciner reactors and the model of the heat exchanger network have been implemented in Engineering Equation Solver (EES) software and they are used to quantify the influence of the variation of storage and release energy fractions in equipment sizing.

3.1. Carbonator model

According to a large number of investigations of the sorption behaviour of solid calcium oxide particles, it has been proven that carbonation conversion of sorbent particles undergoes a drastic fall after a relatively short number of carbonation-calcination cycles [38], [39], [40]. Abanades et al. [38] observed similar decay trends in the CO_2 capture capacity during the carbonation of calcines from natural limestones under a wide range of conditions. Furthermore, Wang et al. [39] suggested that the sintering of sorbents is the possible cause of the decreased activity in CO_2 absorption. In the same way Arias et al. [40] stated that the free surface of the sorbent is reduced during the carbonation/calcination cycles due to sintering and thus the carbonation conversion decays.

Different strategies are proposed to maintain an adequate average sorption capacity of the solid population and a sufficiently high efficiency of the carbonation process. One of these strategies is related to the optimal selection of fresh limestone flowrate or the equivalent stream of purged exhausted material [41]. The low cost of limestone allows the compensation of the CaO sorption degradation by increasing the feed of fresh limestone to the cycle [42].

A *Piaseck* limestone has been taken as a reference for degradation on the sorption capacity with the number of cycles [43]. The conversion of a particle of *Piaseck* limestone after N calcination cycles is calculated through Eq. (8).

$$X_N = \frac{1}{\frac{1}{1-X_r}+k\cdot N} + X_r \quad (8)$$

where k is the deactivation constant with a value of 0.52, X_r the residual conversion that takes a value of 0.075, and N the number of cycles to which the particle has been subjected [43].

However, not all the population of solid sorbent particles have suffered the same number of cycles and an age distribution is found in the solid inventory. There are particles that have just been fed to the system as fresh limestone (N = 0), others that have been carbonated and calcined only once (N = 1) and so on. Therefore, in order to calculate the average sorption capacity of the solid population, the age distribution of the population of sorbent particles must be known. This distribution is represented with the variable r_N and, for an extremely conservative situation in which no solid material is stored in the tanks, it can be calculated through Eq. (9).

$$r_N = \frac{f_p}{\left(1+f_p\right)^N} \quad (9)$$

The variable r_N determines the fraction of CaO particles that circulate between the carbonator and the calciner with a certain number of cycles. The expression can be deduced through successive mass balances for the first cycles, where the CaO purge fraction (f_p), as shown in Eq. (2), is located in calciner [44], [42].

The average conversion of the particle population (X_{ave}) can be calculated using Eq. (10) which uses (i) the fraction of CaO particles (r_N) that have undergone a number of carbonation-calcination N cycles and (ii) the conversion of a sorbent particle (X_N) in the N cycle [37].

$$X_{ave} = \sum_{N=1}^{N=\infty} r_N \cdot X_N \quad (10)$$

Once the average sorption capacity of the particle population is known, the CO_2 capture efficiency can be determined through the CaO/CO_2 molar ratio (R) introduced into the carbonator, as shown in Eq. (3).

3.2. Plant equipment sizing

The sizing of the elements involved in the CaL TCES system strongly depends on the pair of storage and discharge fractions which defines each operation point. Different operating points for each operation mode are determined at steady state, considering CaO purge set at 4% and a constant CaO/CO_2 molar ratio (R) for all operation schemes.

Under energy storage operation mode (ESOM), the energy input (E_{CL}) to the solar calciner is considered to be 100 MWth, while the $CaCO_3$ from the solids separation unit is completely directed to the calciner ($f_{st,CaCO3}$ = 0) by-passing the storage tank of limestone. The operation points analysed for energy storage mode are defined by varying the CO_2 and CaO discharge fraction ($f_{dch,CaO}$) from 0 to 1 for each storage fraction ($f_{st,CaO}$) in a range of 0 to 1, considering increments of 0.1 for each fraction. Each operation scheme under energy storage mode will be defined by a pair of values ($f_{st,CaO}$, $f_{dch,CaO}$). For example, a storage fraction ($f_{st,CaO}$) set to 1 and a discharge fraction ($f_{dch,CaO}$) equal to zero defines an operation scheme in which all the thermal energy available in the solar calciner is stored in the form of CaO and CO_2 and the carbonator is not operated. However, if the storage fraction ($f_{st,CaO}$) drops to 0.7 and the discharge fraction ($f_{dch,CaO}$) is set to 0.1, it means that 70% of the maximum CaO and CO_2 flowrates from the calciner goes directly to its corresponding storage tank; while the remaining 30% is sent to the carbonator together with a 10% of the maximum flow of CaO ($\dot{m}_{st,max,CaO}$) and CO_2 ($\dot{m}_{st,max,CO2}$)

which are discharged from the storage tanks. Therefore, the 40% of the maximum CaO and CO_2 flowrates from the calciner is directly circulated to the carbonator to release energy, while the remaining 60% is stored in their respective tanks. The energy stored under each scenario will depend on the storage and discharge fractions ($f_{st,CaO}$, $f_{dch,CaO}$). Therefore, it is only possible to store or discharge the maximum stored flow of CO_2 and CaO for each energy storage operation point. Furthermore, for a storage fraction ($f_{st,CaO}$) of 0.7, the maximum discharge fraction ($f_{dch,CaO}$) will be 0.7; i.e. the tank never discharges a flowrate higher than the received mass input. A large variety of operating schemes can be obtained under the energy storage operation mode. These schemes allow the generation of operation maps to calculate the required size of heat exchangers and compressor, and the range of energy released in the carbonator (E_{CR}).

Under energy release operation mode (EROM), the maximum power available in the carbonator (E_{CR}) is assumed to be 88.33 MWth as previously justified. The streams of CaO and CO_2 from calciner are fully directed to the carbonator ($f_{st,CaO}$ = 0). The operation schemes are defined by increasing the $CaCO_3$ discharge fraction ($f_{dch,CaCO3}$) from 0 to 1 for each storage fraction ($f_{st,CaCO3}$) in a range of 0 to 1, considering increments of 0.1 for each fraction. Each operation scheme under energy release mode will be defined by a pair of values ($f_{st,CaCO3}$, $f_{dch,CaCO3}$). For example, a storage fraction ($f_{st,CaCO3}$) set to 1 and a discharge fraction ($f_{dch,CacO3}$) equal to zero defines an operation scheme in which solar energy is not available and the calciner must be shut-down; thus the $CaCO_3$ stream from carbonator must be kept in the corresponding storage tank. However, if the storage fraction ($f_{st,CaCO3}$) drops to 0.9 and the discharge fraction ($f_{dch,CaCO3}$) is set to 0.2, it means that 90% of the $CaCO_3$ flowrate from the solids separation unit goes directly to its corresponding storage tank: while the remaining 10% is sent to the calciner together with a 20% of the maximum flow of $CaCO_3$ ($\dot{m}_{st,max,CaCO3}$) which is discharged from the storage tank. Therefore, the 30% of the maximum $CaCO_3$ flowrate from the carbonator is directly circulated to the calciner, while the remaining 70% is stored in its respective tank.

The energy released under each scenario will depend on the storage and discharge fractions ($f_{st,CaCO3}$, $f_{dch,CaCO3}$). Therefore, it is only possible to store or discharge the maximum stored flow of $CaCO_3$ for each energy release operation scheme. In that case, for a storage fraction ($f_{st,CaCO3}$) of 0.9, the maximum discharge fraction ($f_{dch,CaCO3}$) will be 0.9. A large variety of operating schemes can be obtained for the energy release mode. These schemes allow the generation of operation maps to calculate the required size of heat exchangers and compressor, and the range of solar energy required in the calciner (E_{CL}).

The larger number of operation points analysed under both operation modes, the better mapping of the energy requirement or demand operation points.

4. Results and discussion

In this section, the results related to the efficiency of the sorption process taking place in the carbonator and the obtained operation maps are presented. Besides, the analysis of a wide variety of different operation schemes provides an estimation of the size range of the required equipment in the system.

4.1. Average sorbent conversion

The CO_2 capture efficiencies achieved in the carbonator are greater 90% for purged flows, f_p, of 4%. The two parameters that determine the capture efficiency are X_{ave}, a direct function of the purged stream of exhausted material, and the CaO/CO_2 molar ratio, R. The average conversion of the solid material, X_{ave}, is defined by the type of limestone chosen (*Piaseck*) which determines the evolution of sorbent conversion, X_N, with the number of cycles and the age distribution of

solid population, r_N. Under a conservative scenario which does not account for the partial storage of the solid streams leaving the reactors, the average sorption capacity of the particle population using *Piaseck* limestone is X_{ave} of 22.58%. The value set for R is 4.26 which leads to a carbonation conversion efficiency for any operation point of 96.15%. Under that condition, the value given to the purged flow rate of exhausted material determines the maximum CaO and $CaCO_3$ flow at the carbonator outlet (stream 6).

A parametric analysis was carried out to assess the variation of average conversion of the solid population in the solid when the purge of exhausted material and the calcium to carbon dioxide ratio were varied. This variation has a direct effect on the carbon capture efficiency which has been illustrated in Fig. 2. Carbon capture efficiency (η_{capt}) ranges between 13.54% and 100%, Eq. 3, for a solids purge percentage between 1-5% and R values range from 1 to 5.

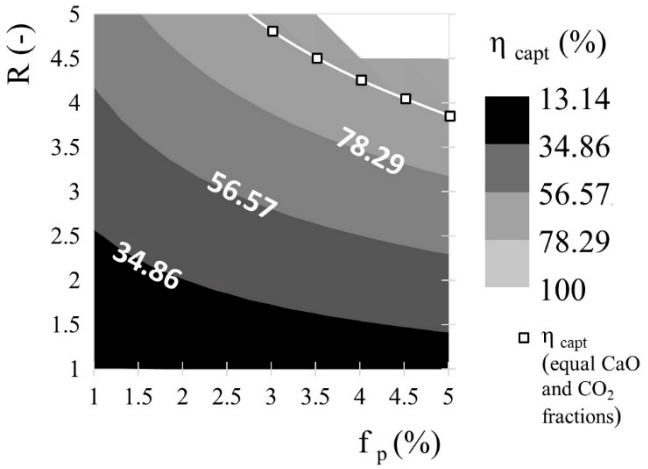

Fig. 2. Carbon capture efficiency in the system for different purged flowrates and CaO/CO_2 ratio.

However, not all the pairs (R, f_p) represented in Fig.2 are suitable for the operation of the CaL-CSP TCES. Only those points located on the white line represented in the figure are adequate for the operation requirements of the system. These points represents those situations in which CO_2 and CaO storage ($f_{st,CO2}$ and $f_{st,CaO}$) are equal as well as discharge ($f_{dch,CO2}$ and $f_{dch,CaO}$) fractions (limitations of the system). In this way, the R value and the average sorbent conversion (X_{ave}) will be kept constant for each operating point within both operating modes (ESOM and EROM).

The lowest carbon capture efficiency is 95.15%, corresponding to a R value of 3.86 and a purge of 5%, while the highest carbon capture efficiency (98.98%) is possible with a purge percentage of 3% and a R ratio of 4.81. Purge percentages (f_p) greater than 5% have not been considered because the increase of the sorbent average activity (X_{ave}) from that value is less sharp. Besides, a R value higher than 5 involves an extremely large solids circulation in the system and therefore the storage volume required is increased. Therefore, an intermediate value of carbon capture efficiency (96.15%) corresponding to a CaO/CO_2 molar ratio (R) of 4.26 and a CaO purge in the calciner (f_p) of 4% has been chosen.

4.2. Operation maps and equipment sizing

The results obtained from the analysed operation points, 100 for each mode of operation, provide relevant information on the size range of the equipment involved in the system.

4.2.1. Storage tank volumes

The maximum flow rates of carbon dioxide and calcium oxide which can be stored have been calculated and these values together with the densities of these substances are used to assess the proper range of the storage tanks. The maximum input flowrate to the CO_2 tank could achieve 24.37 kg/s, while CaO maximum flow could achieve a value of 29.86 kg/s. The storage conditions of the carbon dioxide are 100 ºC and 73 bar which lead to a density of 126.1 kg/m^3. The density of the calcium oxide is 1800 kg/m^3 but considering a void fraction of 30% in the storage tank, the apparent density is around 1260 kg/m^3.

In order to have a preliminary estimation of the maximum CO_2 and CaO storage tank volumes required for the operation of the plant, the most extreme point of operation, load of calciner and the number of hours of operation must be set. The highest load corresponds to the nominal loads, already established as 100 MWth in the calciner. The point of operation for ESOM with larger material storage flow rates corresponds to the calciner operating at nominal load and carbonator off. A parametric analysis of the number of operating hours under limit operation point (ESOM) is carried out to observe the influence on the volumes of the storage tanks, Fig. 3.

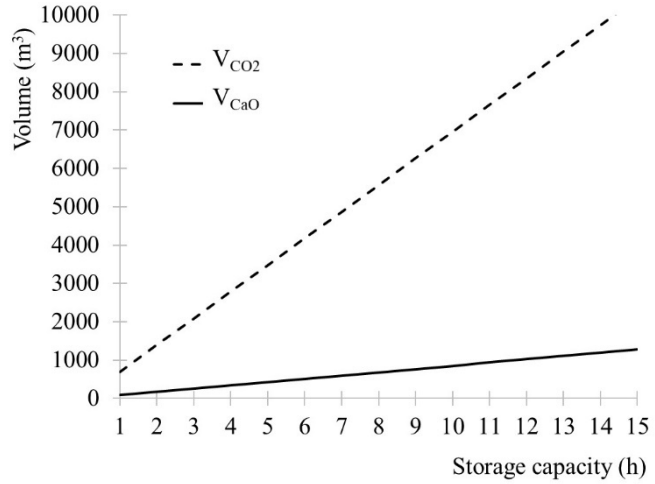

Fig. 3. Volume of the CO_2 and CaO tanks required for maximum storage flow rates vs time.

CaO and CO_2 tank sizes ranges from 85 to 696 m^3 for one hour of storing operation at maximum material storage flow rates, and up to 1,280 – 10,436 m^3 for 15 hours, respectively. This threshold represents a highly improbable situation since the solar calciner will rarely operate at full nominal load during the whole day. The maximum CO_2 storage volume obtained for 15 hours exceeds 10,000 m^3. Although this storage volume represents only a threshold, the information is useful to revise the CO_2 storage conditions to reduce the storage tank size.

4.2.2. Stored power

The maximum potentially stored power under ESOM accounts for the sensible heat of CO_2 and CaO stored and the chemical potential linked to the recarbonation of CaO. The sensible heat amounts to 5.92 MW and the chemical potential that can be later released through the carbonation reaction implies a power of 21.39 MW. However, the maximum energy storage also implies a consumption of the CO_2 compressor of 11.55 MW. On the other hand, the power available in the carbonator (E_{CR}) can range between cero and 88.33 MW, according to the management of the CO_2 and CaO flow streams.

Fig. 4 illustrates the variation of the stored power under a wide range of ESOM operation points. As stated in section 3.2, we assume as a threshold value of the storage or discharge fractions the maximum stored flow rate of CO_2 and CaO for each energy storage operating point. In this way, stored power can be up to 27.31 MW, corresponding to the operating point in which the CaO and CO_2 storage fraction ($f_{st,CaO}$) is maximum and the carbonator does not operate ($f_{dch,CaO}$ = 0). While the minimum energy storage occurs when the carbonator operates at nominal power (88.33 MWth) in ESOM ($f_{st,CaO} = f_{dch,CaO}$) and only the sensible heat of the CO_2 flow that leaves the carbonator towards the storage tank is stored.

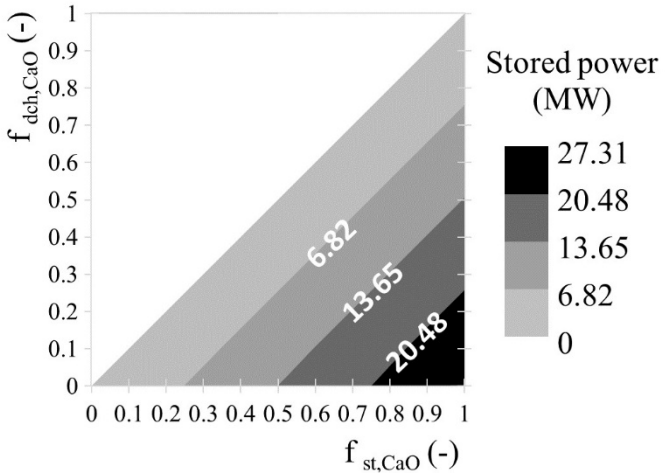

Fig. 4. Stored power under different ESOM points of operation.

The maximum input flow to the $CaCO_3$ tank may achieve a value of 53.29 kg/s and, accounting for the storage temperature of the solid, the maximum power accumulated in the form of sensible heat amounts to 11.68 MW. The solar power range available in the calciner (E_{CL}) can be between cero and 100 MW, the $CaCO_3$ flow stream input will be varied accordingly.

4.2.3. Heat exchangers network

The ranges of exchanged thermal power in each of the Heat Exchangers (HE) are presented in Table 1. The largest heat exchangers are found in the $CaCO_3$ line since these correspond to the highest solid flowrates. The negative sign (-) of the thermal power for a heat exchanger indicates an energy release, while a positive value (+) means that a specific heat exchanger requires an energy input. Under any operating conditions, the total heat losses of each heat exchangers are practically dependent on the storage fractions. The energy losses of the heat exchangers are lower under any EROM operation point since several heat exchangers are by-passed; i.e. all the heat exchangers at the beginning of the CaO (*EE-CaO*) and CO_2 (*EE-*CO_2) storage lines will be disconnected. On the contrary, under ESOM, only the *EE-*$CaCO_3$ heat exchanger, located before the $CaCO_3$ storage tank, will be by-passed.

Table 1. Range size of heat exchangers

Energy flow description		T_{in} (ºC)	T_{out} (ºC)	Q (MW)	
	Heat Exchanger			ESOM	EROM
CO_2	EE-CO_2	950	50	0 to -24.22	0
	EE-CO_2-C	506,9	100	-0.39 to -10.62	-0.39
	EE-CO_2-CR	850	50	-0.82 to 0	-0.82
	ER-CO_2	950 100	850	-3.10 to 20.52	20.52 to -3.10
CaO	EE-CaO	950	200	0 to -20.50	0
	EE-CaO-P	950	200	-0.82	0 to -0.82
	ER-CaO	950 850 200	850	-2.91 to 18.02	18.02 to -2.91
$CaCO_3$	EE-$CaCO_3$	850	200	0	-40.55 to 0
	ER-$CaCO_3$	200	850	0 to 41.38	41.38 to 0

The largest amount of available heat found in the HEN is provided by heat exchanger *EE-$CaCO_3$* which can release up to 40.55 MW of thermal energy as the storage fraction of $CaCO_3$ (stream 7) increases under EROM. The maximum value of thermal energy released by *EE-$CaCO_3$* heat exchanger is achieved when the storage fraction $f_{st,CaCO3}$ is 1 and the flow of $CaCO_3$ leaving the carbonator is stored at 200 ºC. On the contrary, the *EE-$CaCO_3$* heat exchanger is not under operation when the $CaCO_3$ flow rate is fully directed to the calciner, so the $CaCO_3$ storage fraction ($f_{st,CaCO3}$) will be zero.

Another significant heat exchanger is found in the storage line of limestone. The *ER-$CaCO_3$* heat exchanger comes into operation to preheat the flow of $CaCO_3$ discharged from the storage at 200 ºC to 850 ºC. In this case, the heat exchanger designated as *ER-$CaCO_3$* always demands an energy input; up to a maximum of 41.38 MW. *ER-$CaCO_3$* will only be off for specific operation schemes where it is not required to discharge $CaCO_3$ from the storage tank ($f_{dch,CaCO3} = 0$).

The *EE-CO_2* and *EE CaO* heat exchangers belong to the storage line and do not operate when CO_2 and CaO flow rates from calciner are fully directed to carbonator, after passing through *ER-CO_2* and *ER-CaO* heat exchangers, respectively. However, they release thermal energy up to 20.50 and 24.22 MW, respectively, when the storage fraction $f_{st,\,CaO}$ is increased to 1.

The *EE-CO_2-C* and *EE-CO_2-CR* heat exchangers have a minimum threshold of thermal energy released of 0.39 and 0.82 MW, respectively, for any operating point of the energy release operation mode. The *EE-CO_2-C* heat exchanger cools the CO_2 flow before being stored at 100 ºC and 73 bar to take advantage of the temperature reached after compression. The *EE-CO_2-CR* heat exchanger reduces the temperature of the CO_2 flow leaving the carbonator down to 50 °C, for its subsequent compression and storage. The minimum thermal energy released by both heat exchangers is solely related to the storage process of the CO_2 flow from the carbonator (stream 35). However, under the ESOM, the sharper increase of $f_{st,CaO}$, the larger thermal power release

in the *EE-CO_2-C*. This power released in the *EE-CO_2-CR* is reduced to zero if the carbonator does not operate.

The thermal power recovered in the heat exchanger corresponding to the CaO purge (*EE-CaO-P*) presents a constant amount of 0.82 MW when calciner operates at nominal conditions. Although this value can be reduced to zero as the solar energy availability decreases.

Fig. 5 and Fig. 6 illustrate the operation maps of those heat exchangers which can demand or release thermal energy depending on the situation (i.e. storage and discharge fractions and operating loads in calciner and carbonator), the *ER-CO_2* and the *ER-CaO* heat exchangers. These heat exchangers are located before the introduction of CaO and CO_2 streams to the carbonator and their target is to keep the carbonator operation isothermal (850 ºC). The maximum thermal power recovery in these heat exchangers is given when no CO_2 and CaO are discharged from storage ($f_{dch,\ CaO}$). The maximum thermal energy demand occurs when the CO_2 and CaO discharge fraction becomes maximum since both flowrates are required to be preheated from 200 to 850 °C.

In the operation maps shown in Fig. 5 and Fig. 6, a specific operating point for the *ER-CaO* and *ER-CO_2* heat exchangers is highlighted and the values of heat exchanges are presented in the following. Under both operating modes, the selected operating point has a storage fraction of 0.9 and a discharge fraction of 0.1. Under the ESOM, the analysed heat exchangers require a low energy supply, being 1.51 MW for the *ER-CaO* heat exchanger and 1.74 MW for the *ER-CO_2* heat exchanger. While under EROM, both heat exchangers increase their energy demand up to 13.84 MW for the *ER-CaO* heat exchanger and 15.80 MW for the *EE-CO_2* heat exchanger. The lower amount of available solar energy under EROM, the less $CaCO_3$ flowrate from the carbonator diverted to the calciner. The reduction of the $CaCO_3$ flow rate introduced into the calciner implies an increase in the discharge flows of CaO and CO_2 from the storage tanks to keep constant the energy released in the carbonator.

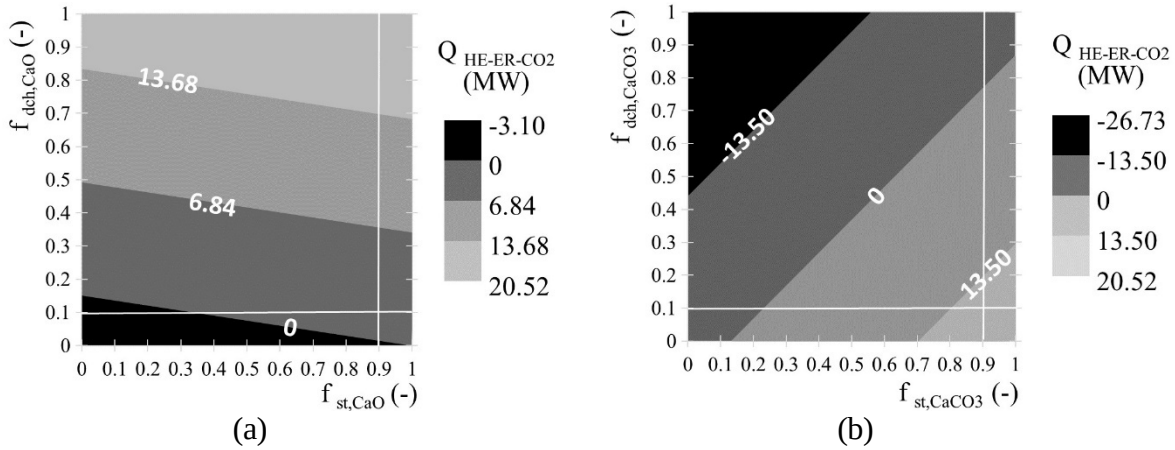

Fig. 5. *ER-CO_2* heat exchanger operation map under ESOM (a) and EROM (b)

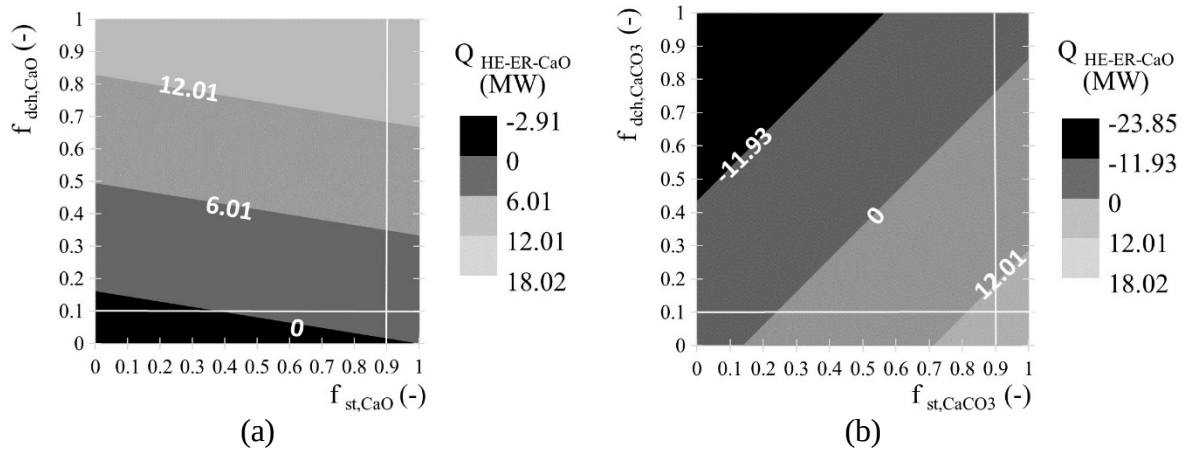

Fig.6. *ER-CaO* heat exchanger operation map under ESOM (a) and EROM (b)

The results obtained for the different operation points studied are shown for a single CaO purge value and the corresponding CaO/CO_2 molar ratio (R) which lead to a constant average conversion of the sorbent (X_{ave}) for any operating point at steady state. Future work including the parametric analysis of these variables and the study of their influence on the amount of stored energy or the energy exchange in the HEN will be of interest.

The analysis of a wide range of operation schemes allows the detailed sizing of the equipment included in the system. From the obtained results, it is observed that some of the largest heat exchangers modify their type of operation (demand or release of heat depending on the operation point under ESOM or EDOM). This information is relevant for the final design of the HEN which will be eventually implemented in the integrated power plant. Further work should be done to develop a methodology which discriminate the operation points which are suitable for a logical operation of these heat exchangers.

5. Conclusion

The novelty of this study relies in the analysis of a wide number of potential points of operation that may take place arising from the different combinations of charge/discharge fractions of the CaO, CO_2 and $CaCO_3$ storage tanks.

In the present work, a large number of operating schemes for a CaL TCES system are evaluated to determine the impact of ESOM and EROM in the sizing of heat exchangers and reactors. The operating limitations of the system increment the dependence between R and f_p reducing the mechanisms to control the carbonation efficiency. Despite this fact, the conversion efficiency in the carbonator exceeds 90% by setting the CaO purge percentage in the calciner at 4%.

Results show that the storage tanks volumes needed for the energy storage could exceed 10,000 m^3 for CO_2 and 1,200 m^3 for lime considering 15 hours of operation at nominal load in the calciner. Besides, the maximum storage power reaches to 27.31 MW when the whole energy from the calciner at nominal load is stored. However, the storage tanks are oversized since the solar calciner will rarely operate at full nominal load during the whole day. Nevertheless, the CO_2 storage conditions should be reviewed to reduce the volume of the CO_2 storage tank and the solids separation at carbonator outlet should be studied in detail as strongly reduces the thermal demand of the system and the size of the storage tank of limestone. This separation process represents a technological challenge that is has not been solved yet. Further research on the

techno-economic feasibility of the solid separation process would be required for the deployment of this storage option.

Operation maps created from the analysed schemes clearly establish the operation points in which power is stored, the amount of stored and released power and the size range of heat exchangers. The maximum power released (40.55 MW) is in the *EE-$CaCO_3$* heat exchanger under the energy release mode, when all the $CaCO_3$ flow from the carbonator is stored. The maximum power demand (41.38 MW) is from the *ER-$CaCO_3$* heat exchanger when it is required to discharge the maximum possible flow of $CaCO_3$ that can be stored. Heat exchangers designated as *EE* always release energy (ESOM and EROM) and heat exchangers called *ER* can release or demand energy depending on the defined storage and discharge fractions. Except for the *ER-$CaCO_3$* heat exchanger that always requires energy to preheat the flow of $CaCO_3$ from 200 ºC to 850 ºC. The discrimination of the operation points which conduct to one or other behaviour of the *ER* heat exchangers is key in the definition of the operation strategy under each mode of operation when the HEN is to be integrated with a power plant.

The main advantage of this study is the analysis of a greater number of operating points under both energy operation modes (storage/release). The number of operating points analyzed is larger than in other studies due to the definition of storage and discharge fractions of CaO, CO_2 and $CaCO_3$. The analysis of these operating points allows to know the power range and the behaviour of the heat exchangers of the plant.

Acknowledgment

The FPU Programme of the Spanish Ministry of Science, Innovation and Universities (FPU 2017/03902) provided financial support for S.P. Ph.D. studies. The research was funded by the EU Horizon 2020 research and innovation programme [GA No 727348], SOCRATCES project. This work has also been supported by Government of Aragon (Research Group DGA T46_17R), co-financed by FEDER 2014-2020 “Construyendo Europa desde Aragón”.

Nomenclature

Symbols

E	released or demand power, MW
f	fraction, -
F	mole flow rate, kmol/s
k	CaO deactivation constant, -
$\dot{m}$	mass flow rate, kg/s
Q	heat flow rate, MW
r	fraction of CaO particles, -
R	molar ratio CaO/CO_2, -
T	temperature, ºC
V	volume, m^3
X	conversion, -
ΔH_R^0	enthalpy of carbonation, kJ/mol
η	efficiency, -

Subscripts and superscripts

0	$CaCO_3$ fresh
ave	average
$capt$	carbon capture
CR	carbonator
CL	calciner
dch	discharge
g	gas
in	input or inlet
max	maximum
N	number of carbonation-calcination cycles
out	output or outlet
p	purge or particle
r	residual
s	solid

st storage

Acronyms and abbreviations

CaL	Calcium-looping	HE	Heat Exchanger
CSP	Concentrating Solar Power	HEN	Heat Exchangers Network
EE	Energy Emitted	SHS	Sensible Heat Storage
EES	Engineering Equation solver	$TCES$	Thermochemical Energy Storage
ER	Energy Required	TES	Thermal Energy Storage

References

[1] Concentrating Solar Power Projects. National Renewable Energy Laboratory 2018. https://solarpaces.nrel.gov/projects (accessed 29 January 2020).

[2] Achkari O, El Fadar A. Latest developments on TES and CSP technologies – Energy and environmental issues, applications and research trends. Appl Therm Eng 2020;167:114806. https://doi.org/10.1016/j.applthermaleng.2019.114806.

[3] Kearney D, Kelly B, Herrmann U, Cable R, Pacheco J, Mahoney R, et al. Engineering aspects of a molten salt heat transfer fluid in a trough solar field. Energy 2004;29:861–70. https://doi.org/10.1016/S0360-5442(03)00191-9.

[4] González-Roubaud E, Pérez-Osorio D, Prieto C. Review of commercial thermal energy storage in concentrated solar power plants: Steam vs. molten salts. Renew Sustain Energy Rev 2017;80:133–48. https://doi.org/10.1016/j.rser.2017.05.084.

[5] Letcher TM. Storing Energy: With Special Reference to Renewable Energy Sources. Elsevier Inc.; 2016. https://doi.org/10.1515/ci-2016-0627.

[6] Chen X, Zhang Z, Qi C, Ling X, Peng H. State of the art on the high-temperature thermochemical energy storage systems. Energy Convers Manag 2018;177:792–815. https://doi.org/10.1016/j.enconman.2018.10.011.

[7] Prieto C, Cooper P, Fernández AI, Cabeza LF. Review of technology : Thermochemical energy storage for concentrated solar power plants. Renew Sustain Energy Rev 2016;60:909–29. https://doi.org/10.1016/j.rser.2015.12.364.

[8] Barker R. The Reactivity of Calcium Oxide Towards Carbon Dioxide and Its Use for Energy Storage. Appl Chem Biotechnol 1974;24:221–7.

[9] Lisbona P, Bailera M, Hills T, Sceats M, Díez LI, Romeo LM. Energy consumption minimization for a solar lime calciner operating in a concentrated solar power plant for thermal energy storage. Renew Energy 2020;156:1019–27. https://doi.org/10.1016/j.renene.2020.04.129.

[10] Ortiz C, Valverde J, Chacartegui R, Perez-Maqueda L. Carbonation of Limestone Derived CaO for Thermochemical Energy Storage: From Kinetics to Process Integration in Concentrating Solar Plants. ACS Sustain Chem 2018;6:6404−6417.

[11] Abanades JC, Rubin ES, Anthony EJ. Sorbent Cost and Performance in CO2 Capture Systems. Ind Eng Chem Res 2004;43:3462–6. https://doi.org/10.1021/ie049962v.

[12] Khosa AA, Xu T, Xia BQ, Yan J, Zhao CY. Technological challenges and industrial applications of CaCO3/CaO based thermal energy storage system – A review. Sol Energy 2019;193:618–636. https://doi.org/10.1016/j.solener.2019.10.003.

[13] Alva G, Lin Y, Fang G. An overview of thermal energy storage systems. Energy 2018;144:341–78. https://doi.org/10.1016/j.energy.2017.12.037.

[14] Sarbu I. A Comprehensive Review of Thermal Energy Storage. MDPI Sustain 2018;10:1–32. https://doi.org/10.3390/su10010191.

[15] Liu D. Progress in thermochemical energy storage for concentrated solar power : A review. Int J Energy Res 2018:1–16. https://doi.org/10.1002/er.4183.

[16] Benitez-guerrero M, Manuel J, Sanchez-jimenez PE, Perejon A, Perez-maqueda LA. Multicycle activity of natural CaCO 3 minerals for thermochemical energy storage in Concentrated Solar Power plants. Sol Energy 2017;153:188–99. https://doi.org/10.1016/j.solener.2017.05.068.

[17] Tregambi C, Salatino P, Solimene R, Montagnaro F. An Experimental Characterization of Calcium Looping Integrated with Concentrated Solar Power. Chem Eng J 2017;331:794–802. https://doi.org/10.1016/j.cej.2017.08.068.

[18] Da Y, Xuan Y, Teng L, Zhang K, Liu X, Ding Y. Calcium-based composites for direct solar-thermal conversion and thermochemical energy storage. Chem Eng J 2020;382:122815. https://doi.org/10.1016/j.cej.2019.122815.

[19] André L, Abanades S. Evaluation and performances comparison of calcium, strontium and barium carbonates during calcination/carbonation reactions for solar thermochemical energy storage. J Energy Storage 2017;13:193–205. https://doi.org/10.1016/j.est.2017.07.014.

[20] Sarrión B, Perejón A, Sánchez-Jiménez PE, Pérez-Maqueda LA, Valverde JM. Role of calcium looping conditions on the performance of natural and synthetic Ca-based materials for energy storage. J CO2 Util 2018;28:374–384. https://doi.org/10.1016/j.jcou.2018.10.018.
[21] Ortiz C, Chacartegui R, Valverde JM, Alovisio A, Becerra JA. Power cycles integration in concentrated solar power plants with energy storage based on calcium looping. Energy Convers Manag 2017;149:815–29. https://doi.org/10.1016/j.enconman.2017.03.029.
[22] Tesio U, Guelpa E, Verda V. Integration of ThermoChemical Energy Storage in Concentrated Solar Power. Part 1: energy and economic analysis/optimization. Energy Convers Manag X 2020:100039. https://doi.org/10.1016/j.ecmx.2020.100039.
[23] Karasavvas E, Panopoulos KD, Papadopoulou S, Voutetakis S. Design of an integrated CSP-calcium looping for uninterrupted power production through energy storage. Chem Eng Trans 2018;70:2131–6. https://doi.org/10.3303/CET1870356.
[24] Ortiz C, Romano MC, Valverde JM, Binotti M, Chacartegui R. Process integration of Calcium-Looping thermochemical energy storage system in concentrating solar power plants. Energy 2018;155:535–51. https://doi.org/10.1016/j.energy.2018.04.180.
[25] Chacartegui R, Alovisio A, Ortiz C, Valverde JM, Verda V, Becerra JA. Thermochemical energy storage of concentrated solar power by integration of the calcium looping process and a CO 2 power cycle. Appl Energy 2016;173:589–605. https://doi.org/10.1016/j.apenergy.2016.04.053.
[26] Tesio U, Guelpa E, Verda V. Integration of ThermoChemical Energy Storage in Concentrated Solar Power. Part 2: comprehensive optimization of supercritical CO2 power block. Energy Convers Manag X 2020;6:100038. https://doi.org/10.1016/j.ecmx.2020.100038.
[27] Karasavvas E, Panopoulos KD, Papadopoulou S, Voutetakis S. Energy and exergy analysis of the integration of concentrated solar power with calcium looping for power production and thermochemical energy storage. Renew Energy 2020;154:743–53. https://doi.org/10.1016/j.renene.2020.03.018.
[28] Bailera M, Lisbona P, Romeo LM, Díez LI. Calcium looping as chemical energy storage in concentrated solar power plants: Carbonator modelling and configuration assessment. Appl Therm Eng 2020:115186. https://doi.org/10.1016/j.applthermaleng.2020.115186.
[29] Bravo R, Ortiz C, Chacartegui R, Friedrich D. Hybrid solar power plant with thermochemical energy storage: A multi-objective operational optimisation. Energy Convers Manag 2020;205:112421. https://doi.org/10.1016/j.enconman.2019.112421.
[30] Koepf E, Alxneit I, Wieckert C, Meier A. A review of high temperature solar driven reactor technology: 25 years of experience in research and development at the Paul Scherrer Institute. Appl Energy 2017;188:620–51. https://doi.org/10.1016/j.apenergy.2016.11.088.
[31] Zsembinszki G, Sole A, Barreneche C, Prieto C, Fernández AI, Cabeza LF. Review of reactors with potential use in thermochemical energy storage in concentrated solar power plants. Energies 2018;11. https://doi.org/10.3390/en11092358.
[32] Karasavvas E, Panopoulos KD, Papadopoulou S, Voutetakis S. Study of a drop-tube carbonator reactor for CSP-calcium looping based on a heterogeneous reaction model. Chem Eng Trans 2019;76:877–82. https://doi.org/10.3303/CET1976147.
[33] Yan Y, Wang K, Clough PT, Anthony EJ. Developments in calcium/chemical looping and metal oxide redox cycles for high-temperature thermochemical energy storage: A review. Fuel Process Technol 2020;199:106280. https://doi.org/10.1016/j.fuproc.2019.106280.
[34] Rinaldi F, Binotti M, Giostri A, Manzolini G. Comparison of linear and point focus collectors in solar power plants. Energy Procedia 2013;49:1491–500. https://doi.org/10.1016/j.egypro.2014.03.158.
[35] European Commission. PVGIS - Photovoltaic geographical information system 2019.
[36] Chacartegui R, Alovisio A, Ortiz C, Valverde JM, Verda V, Becerra JA. Thermochemical energy storage of concentrated solar power by integration of the calcium looping process and a CO2 power cycle. Appl Energy 2016;173:589–605. https://doi.org/10.1016/j.apenergy.2016.04.053.
[37] Rodriguez N, Alonso M, Grasa G, Abanades JC. Heat requirements in a calciner of CaCO3 integrated in a CO2 capture system using CaO. Chem Eng J 2008;138:148–54. https://doi.org/10.1016/j.cej.2007.06.005.
[38] Abanades JC, Alvarez D. Conversion limits in the reaction of CO2 with lime. Energy and Fuels 2003;17:308–15. https://doi.org/10.1021/ef020152a.
[39] Wang J, Anthony EJ. On the Decay Behavior of the CO2 Absorption Capacity of CaO-Based Sorbents. Ind Eng Chem Res 2005;44:627–9. https://doi.org/10.1021/ie0493154.
[40] Arias B, Abanades JC, Grasa GS. An analysis of the effect of carbonation conditions on CaO deactivation curves. Chem Eng J 2011;167:255–61. https://doi.org/10.1016/j.cej.2010.12.052.
[41] Romeo LM, Lara Y, Lisbona P, Escosa JM. Optimizing make-up flow in a CO2 capture system using CaO. Chem Eng J 2009;147:252–8. https://doi.org/10.1016/j.cej.2008.07.010.
[42] Martínez A, Lara Y, Lisbona P, Romeo LM. Energy penalty reduction in the calcium looping cycle. Int J

Greenh Gas Control 2012;7:74–81. https://doi.org/10.1016/j.ijggc.2011.12.005.
[43] Grasa GS, Abanades JC. CO $_2$ Capture Capacity of CaO in Long Series of Carbonation/Calcination Cycles. Ind Eng Chem Res 2006;45:8846–51. https://doi.org/10.1021/ie0606946.
[44] Abanades JC. The maximum capture efficiency of CO2 using a carbonation/calcination cycle of CaO/CaCO3. Chem Eng J 2002;90:303–6. https://doi.org/10.1016/S1385-8947(02)00126-2.